ARTICLE

www.the-innovation.org

Sahara's surface transformation forced an abrupt hydroclimate decline and Neolithic culture transition in northern China

Yandong Hou,[1] Hao Long,[1,*] Sumiko Tsukamoto,[2] Zhengyao Lu,[3] Jie Chen,[4,5] Daniel E. Ibarra,[6] Toru Tamura,[7,8] Qiong Zhang,[9] Weiyi Sun,[10] Jingran Zhang,[10] Lei Gao,[1] Manfred Frechen,[2] and Ji Shen[11]

*Correspondence: longhao@niglas.ac.cn

Received: February 2, 2023; Accepted: November 29, 2023; Published Online: November 30, 2023; https://doi.org/10.1016/j.xinn.2023.100550

GRAPHICAL ABSTRACT

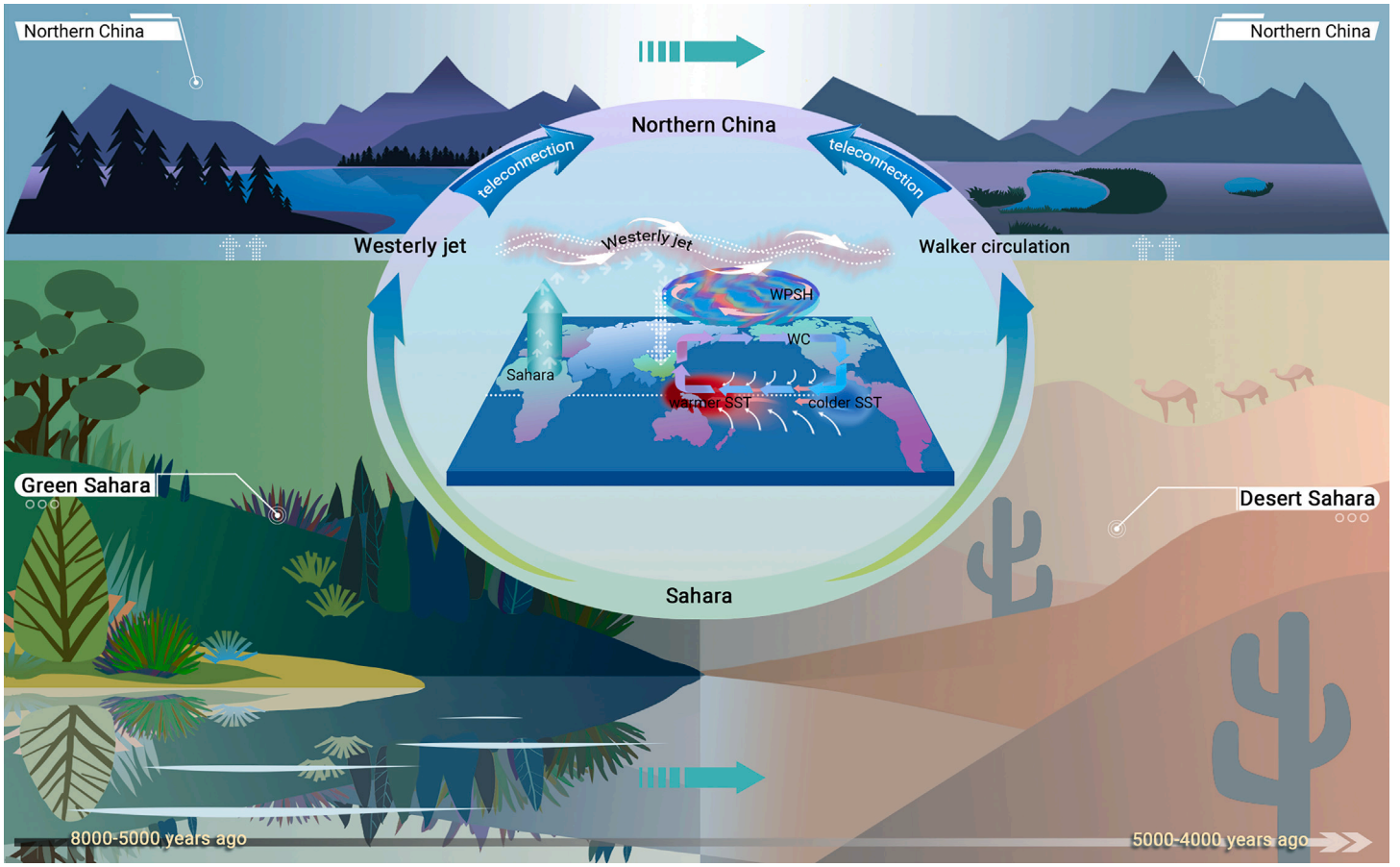

PUBLIC SUMMARY

- Holocene rainfall variations were quantified with energy balance model on lake-levels.
- An abrupt hydroclimate decline in northern China occurred 5,000–4,000 years ago.
- This abrupt change event may trigger shifts in Neolithic cultures in northern China.
- Simulations suggest the impact of the end of Green Sahara on rainfalls of East Asia.

ARTICLE

Sahara's surface transformation forced an abrupt hydroclimate decline and Neolithic culture transition in northern China

Yandong Hou,[1] Hao Long,[1,*] Sumiko Tsukamoto,[2] Zhengyao Lu,[3] Jie Chen,[4,5] Daniel E. Ibarra,[6] Toru Tamura,[7,8] Qiong Zhang,[9] Weiyi Sun,[10] Jingran Zhang,[10] Lei Gao,[1] Manfred Frechen,[2] and Ji Shen[11]

[1]State Key Laboratory of Lake Science and Environment, Nanjing Institute of Geography and Limnology, Chinese Academy of Sciences (NIGLAS), Nanjing 210008, China
[2]Leibniz Institute for Applied Geophysics (LIAG), Department of Geochronology, 30655 Hannover, Germany
[3]Department of Physical Geography and Ecosystem Science, Lund University, 22100 Lund, Sweden
[4]Key Laboratory of Western China's Environmental Systems (Ministry of Education), College of Earth and Environmental Sciences, Lanzhou University, Lanzhou 730000, China
[5]College of Atmospheric Sciences, Lanzhou University, Lanzhou 730000, China
[6]Institute at Brown for Environment and Society and Department of Earth, Environmental, and Planetary Sciences, Brown University, Providence, RI 02912, USA
[7]Geological Survey of Japan, National Institute of Advanced Industrial Science and Technology, Tsukuba, Ibaraki 305-8567, Japan
[8]Graduate School of Frontier Sciences, University of Tokyo, Kashiwa, Chiba 277-8561, Japan
[9]Department of Physical Geography and Bolin Centre for Climate Research, Stockholm University, 10691 Stockholm, Sweden
[10]School of Geography, Nanjing Normal University, Jiangsu Centre for Collaborative Innovation in Geographical Information Resource Development and Application, Key Laboratory of Virtual Geographic Environment, Ministry of Education of China, Nanjing 210023, China
[11]School of Geography and Ocean Science, Nanjing University, Nanjing 210023, China
*Correspondence: longhao@niglas.ac.cn

Received: February 2, 2023; Accepted: November 29, 2023; Published Online: November 30, 2023; https://doi.org/10.1016/j.xinn.2023.100550

Citation: Hou Y., Long H., Tsukamoto S., et al., (2024). Sahara's surface transformation forced an abrupt hydroclimate decline and Neolithic culture transition in northern China. The Innovation **5(1)**, 100550.

The remote forcing from land surface changes in the Sahara is hypothesized to play a pivotal role in modulating the intensity of the East Asian summer monsoon (EASM) through ocean-atmospheric teleconnections. This modulation has far-reaching consequences, particularly in facilitating societal shifts documented in northern China. Here, we present a well-dated lake-level record from the Daihai Lake Basin in northern China, providing quantitative assessments of Holocene monsoonal precipitation and the consequent migrations of the northern boundary of the EASM. Our reconstruction, informed by a water-and-energy balance model, indicates that annual precipitation reached ~700 mm during 8–5 ka, followed by a rapid decline to ~550 mm between 5 and 4 ka. This shift coherently aligns with a significant ~300 km northwestward movement of the EASM northern boundary during the Middle Holocene (MH), in contrast to its current position. Our findings underscore that these changes cannot be entirely attributed to orbital forcing, as corroborated by simulation tests. Climate model simulations deployed in our study suggest that the presence of the Green Sahara during the MH significantly strengthened the EASM and led to a northward shift of the monsoon rainfall belt. Conversely, the Sahara's reversion to a desert landscape in the late Holocene was accompanied by a corresponding southward retraction of monsoon influence. These dramatic hydroclimate changes during ~5–4 ka likely triggered or at least contributed to a shift in Neolithic cultures and societal transformation in northern China. With decreasing agricultural productivity, communities transitioned from millet farming to a mixed rainfed agriculture and animal husbandry system. Thus, our findings elucidate not only the variability of the EASM but also the profound implications of a remote forcing, such as surface transformations of the Sahara, on climatic changes and cultural evolution in northern China.

INTRODUCTION

The abrupt shifts in Earth's climate, especially those instigating nonlinear feedbacks such as vegetation-climate interaction, can trigger widespread ecosystem transitions, leading to the potential for significant cultural disruption.[1] This effect is particularly conspicuous in the region influenced by the East Asian summer monsoon (EASM), a powerful climate system known for its influence on societal changes.[2] A wealth of archaeological data demonstrates that even minor variations in the intensity and duration of the EASM can have profound societal and economic effects on millions of individuals each year.[3]

A key feature of the EASM is its northern boundary, which constitutes a critical climatological demarcation defined by the northernmost reach of monsoon precipitation.[4] The boundary of the EASM is defined as the northern limit of monsoon precipitation, where the difference between local summer (May–September) and winter (November–March) precipitation rates exceeds 2 mm day^{-1}, and summer precipitation constitutes >55% of the annual precipitation.[5] In climatological terms, the northern boundary is defined as the May–September precipitation (300 mm precipitation isoline) in models[6] (Figure 1). Geographically, the northern boundary of the monsoon is parallel or close to the 400 mm year^{-1} precipitation isoline.[7] The region proximate to this boundary is especially sensitive to climatic changes and offers invaluable insights into the interplay between climate shifts and societal transformations. Located near the boundary of the EASM, northern China embodies this dynamic interplay. At the site of significant societal developments during the Neolithic and Bronze Ages, it serves as a unique and informative case study for investigating the influences of climate variability on human societies.[8–10] By scrutinizing such sensitive regions, our understanding of the broad-ranging effects of climatic shifts on society may be enriched significantly.

The EASM, renowned for its complexity and societal effects, has been the subject of extensive research. Paleoclimate records have played a crucial role in enriching our understanding of the variability patterns and driving mechanism of the EASM throughout the Holocene.[18] Particularly during the Middle Holocene (MH), multiple studies provide compelling evidence that the EASM boundary extended further north than its present limit. Yang et al. used precisely dated tree-ring stable isotopes to infer a significant northwestward extension of the EASM boundary by at least 300 km northwest compared to its current position.[2] Complementary findings from lacustrine sediments in northeastern China[7] and plant biomass data from loess sections across the Chinese Loess Plateau[19] suggested a northwestward displacement of the EASM rain belt by 300–400 km during the Early Holocene (EH) and MH.

Despite compelling evidence from paleoclimate archives, climate models generally struggled to reproduce substantial expansion of the northern boundary of the EASM during the MH. Simulations from the Palaeoclimate Modelling Intercomparison Project3 (PMIP3) and the Transient Climate Evolution-21 ka (TraCE-21 ka) experiments indicates a relatively modest northwestward migration of the EASM boundary by 100–150 km from the pre-industrial (PI) to the MH.[16,20] These models mainly incorporate orbital insolation as variable boundary conditions over the last 6 ka and often overlook significant environmental changes, such as the dramatic land surface transformation of the Sahara. During the EH and HM, the Sahara was a lush landscape, often referred to as the Green Sahara, with significantly lower dust emissions compared to today[21] and transitioned to a desert in the Late Holocene (LH).[3] This dramatic transformation is believed to have a significant impact on the intensity and duration of the EASM in northern China.[15] However, the precise link between the magnitude and spatial extent of the EASM and various vegetation-induced feedbacks in the Saharan area remains elusive. This uncertainty can be partially attributed to a lack of suitable proxies that facilitate a comprehensive evaluation of the impact of Green Sahara and its end on the EASM marginal area during the Holocene.

Our study aims to investigate the connection of the end of Green Sahara to the abrupt hydroclimate changes in northern China, along with their subsequent societal consequences. Given its high sensitivity to the migration of the EASM rainfall belt and a rich history of cultural developments, northern China serves as an

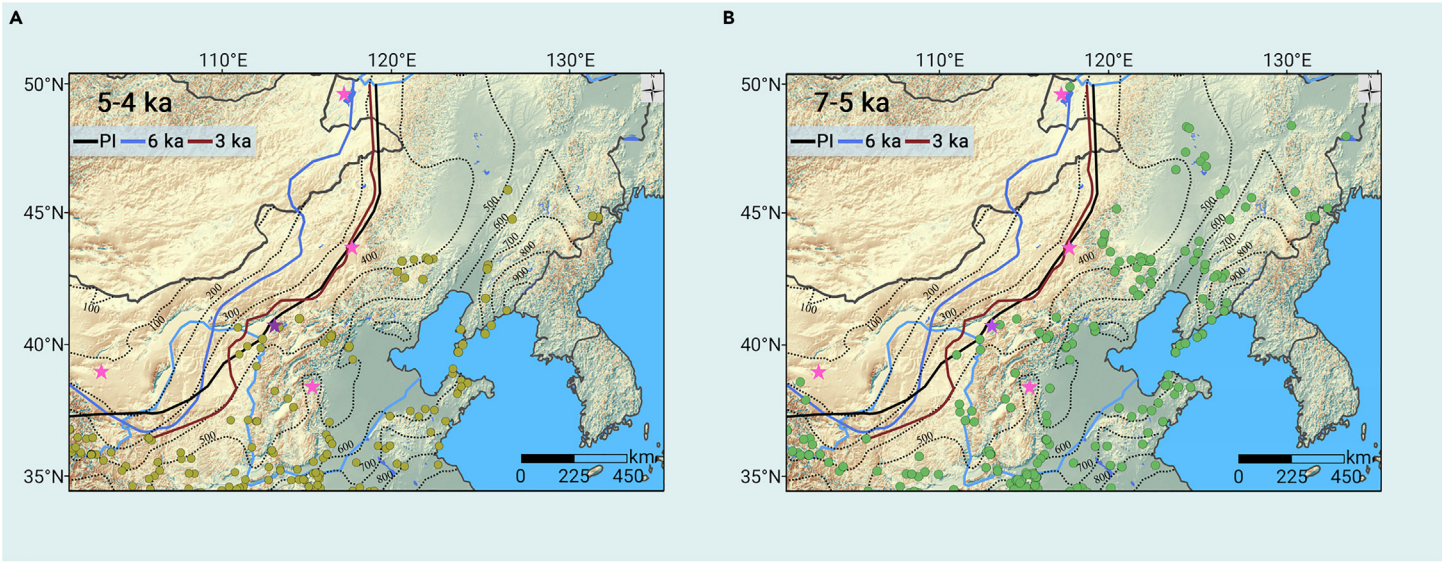

Figure 1. Locations of Daihai Lake, Hulun Lake, Daili Lake, and Baijian Lake and spatiotemporal distribution of archaeological sites in northern China Radiocarbon dates from Neolithic archeological sites are between 7 and 5 ka (A) and 5 and 4 ka (B).[11–14] The mean position of the EASM northern boundaries is in the PI (black solid line),[15] 3 ka (red solid line),[16] and 6 ka (blue solid line).[15] A climatological northern boundary is defined as the May–September precipitation (300 mm precipitation isoline) in model stimulation.[17]

ideal region to explore this teleconnection relationship. In this study, we use a combination of luminescence dating techniques, proxy data, and a hydrological model to reconstruct the historical water level of Daihai Lake and the precipitation patterns of the Holocene. Our results depict a time line in which annual precipitation reached up to ~700 mm between 8 and 5 ka, sufficient to maintain a high stand of Daihai Lake. However, an abrupt decrease to ~550 mm is observed at ~5–4 ka, aligning with the end of the Green Sahara. These findings suggest that the drastic climatic changes accompanying the end of the Green Sahara may have a significant influence on the Neolithic cultures in northern China. Notably, we discern two key consequences: (1) hydrologic instability in culture relicts, which became more susceptible to megadroughts due to their proximity to the northern boundary of the EASM, and (2) reduced social resilience as millet cultivation, a vital agricultural resource, was adversely affected. This led to a shift toward intensified pastoralism in response to the ~150-mm decrease in precipitation and substantial declines in agricultural productivity.

RESULTS

We investigated four outcrops located in the western and eastern parts of the Daihai Lake Basin, with the chronostratigraphy of these four profiles illustrated in Figure 2. The onset of fluvial deposition occurred during the EH (11.3 ± 0.9 ka) in the sedimentary sequence DH18-3. The presence of a fluvial environment between 13.0 and 8.3 ka indicates that the lake level was below ~1,259 m during this period. Notably, this fluvial deposition took place in an area currently incised, exposing the DH18-3 section, indicating that the lake level was higher than its present-day level. Further chronological evidence supporting this lower lake level during the EH comes from the DH17-1 section, with an evident depositional hiatus between

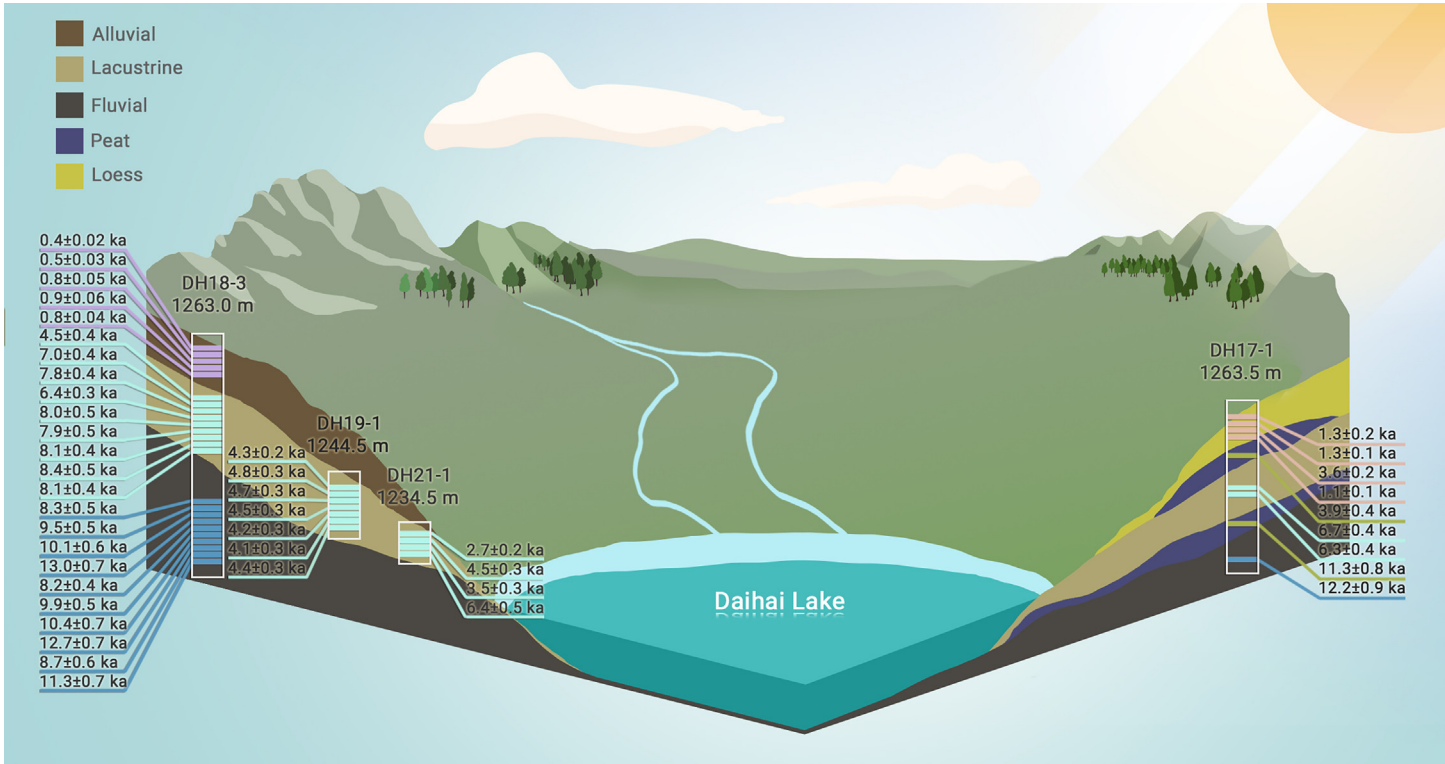

Figure 2. Stratigraphy and chronology of sampling sections in Daihai Lake Basin

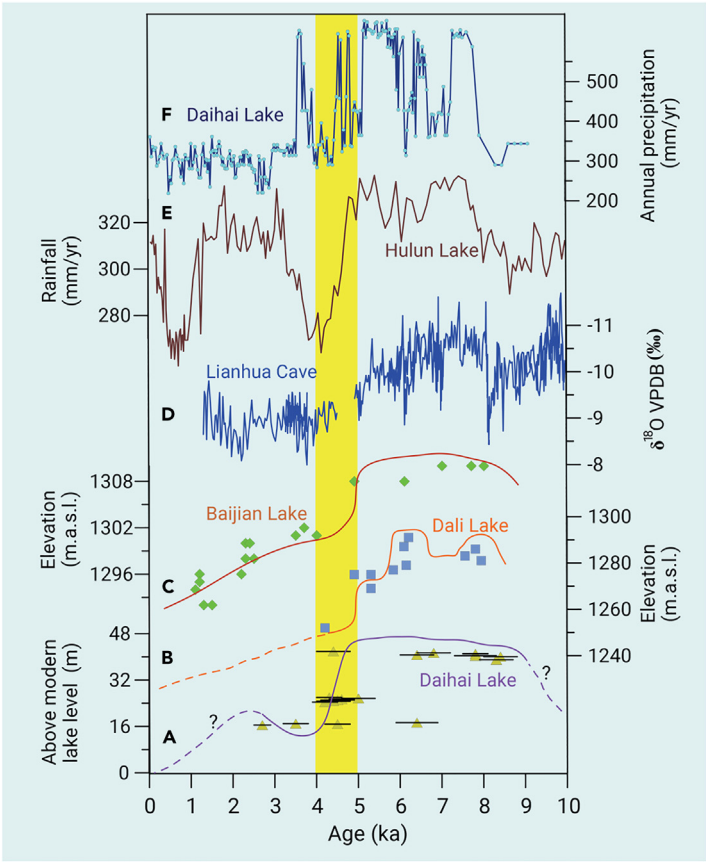

Figure 3. A widespread weakening of EASM in northern China at 5–4 ka (A) Lake-level changes at Daihai Lake (this study); (B and C) lake-level fluctuations of Daili Lake and Baijian Lake[7,28]; (D) $\delta^{18}O$ records from Lianhua Cave[30]; (E and F) quantitative precipitation reconstruction based on pollen data from lake cores from Hulun Lake and Daihai Lake.[26,29] Yellow vertical color bar indicates the transition from wet to dry conditions between 5.0 and 4.0 ka.

~10 and 7 ka at a similar elevation of ~1,259 m. Following this, lacustrine deposits indicate a lake transgression at 8.3 ± 0.5 ka at an elevation of ~1,260 m in DH18-3. Throughout the MH, from ~8.3 to 4.5 ka, we infer stable and highest lake levels from 9 lacustrine sediment samples positioned between 1,260 m and 1,259 m (~42 m higher than the present lake level). Additional sediment samples from DH17-1 and DH19-1 also reflect high lake-level conditions during this period. Conversely, the sedimentary gap observed in lacustrine deposits between ~4.5 and ~0.8 ka, similar to the absence of deposition in DH19-1 after 4 ka, suggests a subsequent reduction in lake levels, with at least a 20-m drop inferred from the elevation difference between DH18-3 and DH19-1. More specifically, a ~26-m decline in lake level at 5–4 ka is confirmed by the lacustrine sediment between DH21-1 and DH18-3. Moreover, the abrupt shift from lacustrine sediment to peat deposition in the DH17-1 section at ~3.9 ka may represent a lake regression. The subsequent loess deposition suggests a continued retreat of the lake during LH, with the lake level likely significantly below 1,262 m, allowing for dust deposition on the shore. In the DH18-3 profile, 5 luminescence ages of alluvial deposits (at elevations between 1,260 and 1,263 m) suggest that the lake continued to descend after 0.9 ka, remaining at a relatively low level. It is worth noting that the water in Daihai Lake rose to slightly higher levels before falling back to its present level during ~2.7 ka, as demonstrated by the existence of lacustrine sediment in the DH21-1 profile at an elevation of ~1,234 m. We conclude that the lake experienced a high lake level at MH (~42 m above the modern lake level), followed by a significant lake regression ~5–4 ka, signifying a drop of at least 26 m.

DISCUSSION

Assessment of impact on lake water fluctuations and quantitative reconstruction of Holocene precipitation

To assess the factors influencing lake level fluctuations, we used a water-and-energy balance model that incorporates climate variables to simulate lake areas. The model is represented by Equation 1:

$$Pk_{run}(A_B - A_L) + PA_L = E_L A_L \quad \text{(Equation 1)}$$

In this equation, P represents precipitation, k_{run} is a coefficient determining the fraction of P converted to runoff, A is the area (subscripts: B, closed basin area; L, lake area), and E_L is lake evaporation. To directly quantify the relationship between precipitation and runoff under varied climatic conditions, we applied the Budyko curve[22,23] to determine k_{run}, as shown in Equation 2:

$$1 - k_{run} = \frac{ET}{P} = 1 + \frac{E_P}{P} - \left(1+\left(\frac{E_P}{P}\right)^{\omega}\right)^{\frac{1}{\omega}} \quad \text{(Equation 2)}$$

Here, ET is evapotranspiration, E_P denotes potential evapotranspiration, and ω is a free parameter that represents the integrated effects of catchment attributes. We tested the sensitivity of lake level changes to the input variables, including air temperature and precipitation (as detailed in Text S5). Both precipitation and temperature values were increased by factors ranging from 1.0 to 2.0 in intervals of 10%–20% of the modern value. We determined the ω value as 2.6. We found the ratio A_L:A_B (lake area to closed basin area) was notably more sensitive to changes in precipitation than temperature. For instance, a 50% increase in precipitation resulted in a change in the A_L:A_B ratio from 3% to 13%. In contrast, a 50% increase in temperature leads to a small decrease in the A_L:A_B ratio from 3%–1.5%. Therefore, the A_L:A_B ratio exhibits greater sensitivity to changes in precipitation than temperature.

The precipitation values required to sustain specific lake levels during different Holocene periods were deduced by combining Equations 1 and 2. To recreate the paleohydrology of the lake from 8 to 4 ka, we used a digital elevation model to reconstruct the area of the lake, taking into account the reconstructed lake levels and a plausible range of lake evaporation rates, following the approach of Goldsmith et al.[7] (Figure S12).

The results suggest that maintaining the highstands of lake levels during the MH would necessitate an annual precipitation of ~700 mm, whereas sustaining lake levels during the 5- to 4-ka period could require lower precipitation values, as low as 550 mm (Figure S13). Considering the current spatial distribution of rainfall in continental China (Figure 1), an increase of 300 mm in annual precipitation could correspond to a northwestern expansion of the EASM-influenced region by ~300–400 km.

Abrupt decline of EASM during 5–4 ka

The most striking observation from our reconstructed lake level is a sudden drop of ~26 m, reflecting a reduction of 150 mm in precipitation during 5–4 ka. This abrupt change in lake level suggests a weakening of the EASM during this period, an inference reinforced by other palaeoclimatic proxies in northern China, especially near the proximity to the northern boundary of the EASM. Several previous studies based on sediment cores from Daihai Lake have provided detailed information on hydroclimate changes since the late deglaciation.[24–26] Concentrations of total organic carbon in the DH99 core sediments showed below-average values at the interval of 4.1–3.8 ka, indicating reduced precipitation.[27] Pollen-based quantitative climate reconstructions from Daihai Lake also indicated a cold and dry event occurring at ~4.5–4.0 ka, further strengthening the evidence of decreasing precipitation[24,26] (Figure 3A). Concurrent fluctuations in lake-level fluctuations, such as a ~40-m decline at ~5.0–4.0 ka, have been observed in Dali Lake, indicating an abrupt termination of the Holocene humid period with significant effects on Chinese culture[7] (Figure 3B). Baijian Lake also demonstrated a highstand phase during the MH period, followed by a sudden ~10-m drop between 5 and 4 ka[28] in the context of low-relief basin morphology (Figure 3C). Further corroborating this trend, a quantitative paleoclimatic reconstruction from Hulun Lake in northeastern Inner Mongolia showed exceptionally dry and relatively cold conditions between 4.4 and 3.4 ka.[29] In the northeastern Tibetan Plateau, tree-ring-based analysis revealed a rapid decrease in moisture availability between 4.0 and 3.5 ka, transitioning to a dry hydroclimatic regime, with mean precipitation estimated to be 42% ± 4% lower than that of the MH period.[2] However, high-resolution and well-chronologically resolved speleothem $\delta^{18}O$ data from Lianhua Cave in northern China (Figure 3D) indicated a prominent hiatus from 5.0 to 4.5 ka.[30] These collective findings affirm our conclusion that the EASM weakened in northern China during 5–4 ka, which is in line with our investigations from the Daihai Lake Basin.

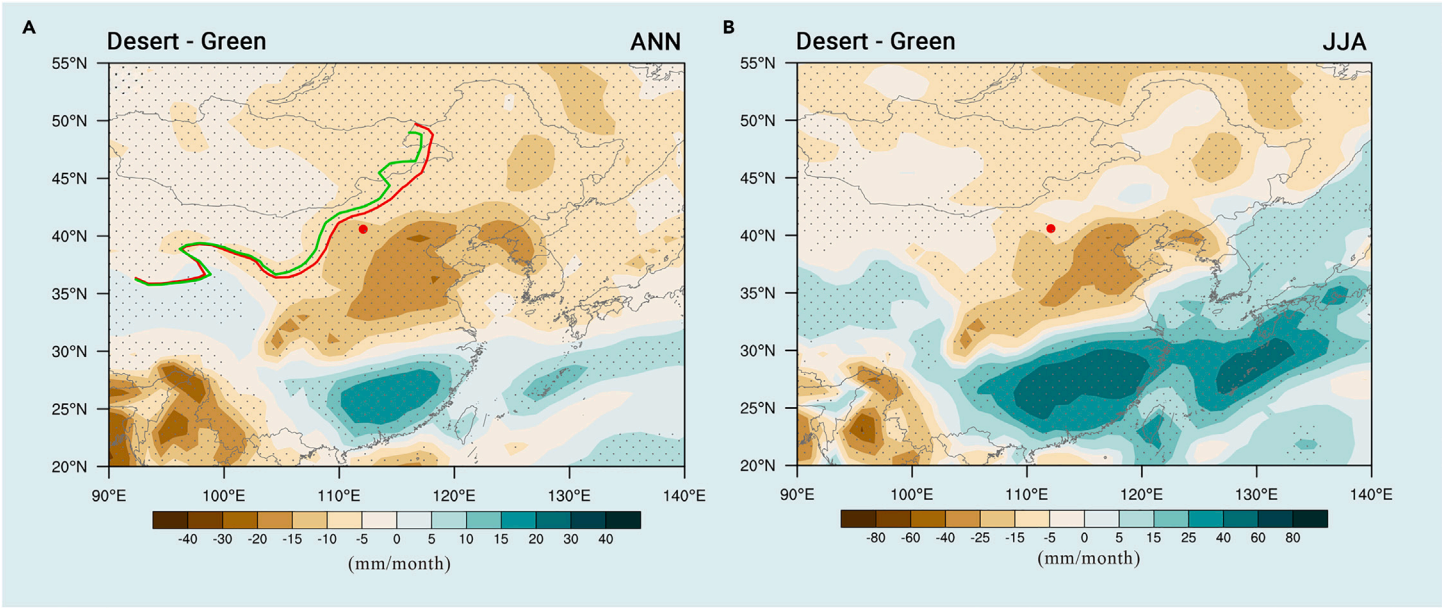

Figure 4. Numerical simulation of precipitation in northern China Annual mean precipitation (A) and summer precipitation (B) anomalies (mm/month) under the effect of end of Saharan vegetation (MH_{Desert}–MH_{Green}). The mean position of the EASM northern boundaries are Green Sahara (green solid line) and the end of Green Sahara (red solid line). The red dot denotes the location of Daihai Lake. ANN, annual.

Possible forcing mechanisms related to the end of Green Sahara

Our study indicates a 300-km northward shift in the northern boundary of the EASM during the MH, corroborating previous proxy records.[2,7,19] Interestingly, this suggests a more extensive northward migration of the EASM boundary than that inferred from modeling results based on TraCE-21 ka and PMIP3 model results.[16,20] It should be noted that these modeling studies define the climatological northern boundary based on precipitation from May to September,[6] whereas the proxies used for precipitation reconstruction encompass the entire year (January–December). In fact, in northern China, approximately 80% of the mean annual precipitation in northern China falls between June and September.[24] The substantial discrepancy between the model and data suggests that models may not be capturing some crucial processes. However, simulations incorporating land surface feedbacks in the Sahara region reproduced more extensive magnitude and northward extent of the EASM.[6,15] For instance, Chen et al.[6] demonstrated that orbital forcing shifts the simulated northern boundary of the EASM by up to 213 km, with an additional northwestward shift of up to 90 km when considering the greening of the Sahara. Similarly, Piao et al.[15] found that the northward extension reached 155 km and 362 km during the MH, when considering orbital forcing alone and combined orbital and Green Sahara forcing, respectively. Therefore, our reconstructed ~300 km northern migration of the EASM northern boundary during the MH aligns well with these simulations when taking into account the remote influence of the Green Sahara.

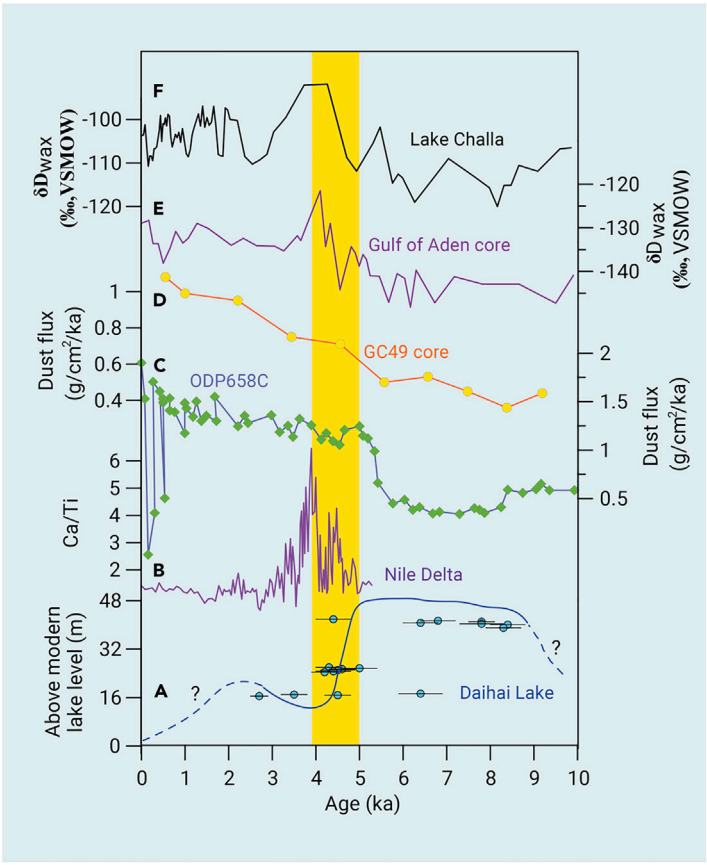

Figure 5. Comparison of the lake-level changes of Daihai Lake with the end of the Green Sahara (A) Lake-level changes at Daihai Lake in present study; (B) Ca/Ti record of dust deposition in the Nile Delta[34]; (C and D) terrigenous dust flux records from cores GC66 and ODP Site 658C[21,32]; (E and F) δD_{wax} records from Lake Challa[35] and marine core P178–15P.[36] Yellow vertical color bar indicates the transition from a wet to a dry condition between 5.0 and 4.0 ka.

Our study suggests that a reduction of ~150 mm in annual precipitation is likely associated with a 150-km southward migration of the EASM during the 5–4 ka period. This result aligns well with modeling findings, which propose a southeastward migration of the EASM rain belt by ~200 km when combining results from the TraCE-21 ka and EC-Earth[15,16] (Figure 1). Furthermore, a sensitivity experiment (MH_{Desert}–MH_{Green}) considers reduced vegetation and increased dust in the Sahara region at the end of the Green Sahara, inferring the response of precipitation in northern China to these remote changes. As the Sahara transitioned from a green state to a desert state, the center of reduced precipitation anomalies, characterized by a reduction of ~40 mm/month, was found in northern China (Figure 4A), which is consistent with our reconstructed results. Historically, the widespread drought in northern China has often been linked to the rapid cooling of the North Atlantic, known as Holocene Event 3, characterized by increased ice-rafted debris.[27] However, the magnitude of this event was overshadowed in comparison to other Holocene ice-rafting events that did not align with large-scale megadroughts.[31] Furthermore, that no significant centennial-scale weakening of the EASM occurred at 4.2 ka was revealed by high-resolution speleothem $\delta^{18}O$ records from the Lianhua Cave from northern China.[30] Similarly, the MH-length hydroclimate reconstruction based on precisely dated tree rings on the northeastern Tibetan Plateau also did not indicate a significant transition in the hydroclimate at ~4.2 ka in northern China.[2] Thus, rather than attributing this event to orbital forcing changes, we propose that it was likely driven by

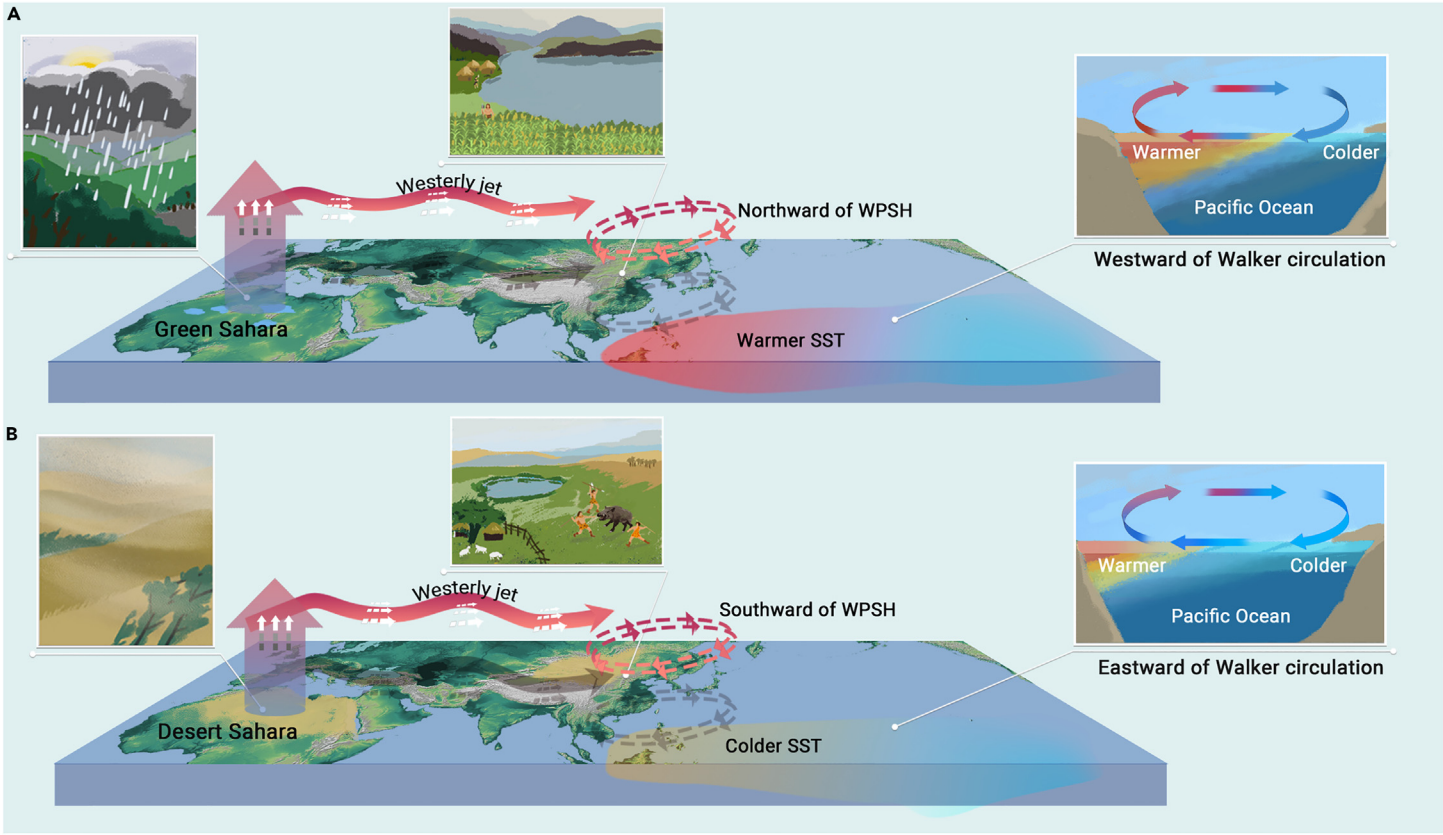

Figure 6. Schematic representation of the mechanisms behind the changes in EASM variability Changes in landscapes, westerly jet, WPSH, and Walker circulation between Green Sahara (A) and the end of Green Sahara (B).

feedback mechanisms triggered by shifts in land surface changes following the Green Sahara termination. This theory accounts for the nonlinearity of the event, which contrasts with the gradual changes that are typically associated with orbital forcing.

We found a clear weakening trend in the EASM over northern China, particularly near its northern boundary of the EASM, between 5.0 and 4.0 ka. This trend coincides with an abrupt increase in dust emissions from the Saharan area (Figure 5). The shift from humid to arid conditions aligns closely with an abrupt increase in aeolian dust supply during the MH (Figure 5C), observed at Ocean Drilling Project (ODP) Site 658C off Cap Blanc, Mauritania at ~5.5 ka.[32] Likewise, reconstructions of aeolian dust accumulation in sediments from the northwestern African margin suggest abrupt and synchronous changes in dust fluxes across all cores at the onset and end of the Green Sahara at~4.9 ka[21] (Figure 5D). A prominent dust layer identified at 4.0 ka within Kilimanjaro ice in eastern equatorial Africa, suggests a significant climate shift and the end of the Green Sahara.[33] Data on the Ca/Ti ratio in dust deposition records from the Nile Delta indicates an increase in windblown dust entering the Nile system (Figure 5B), signifying a prevalent dry period around the end of the Green Sahara at 4.0 ka.[34] Moreover, a decline in the eastern and western African rainfall inferred from the hydrogen isotopic composition of leaf waxes (δD_{wax}) is also centered at ~5.0 ka and ~4.1 ka[35,36] (Figures 5E and 5F). Therefore, we suggest that an abrupt decrease in monsoon rainfall in the EASM during 5–4 ka is probably associated with the failure of African monsoon at the end of the Green Sahara.

Through the effect of the Green Sahara and the reduction in dust, the precipitation of the Northern Hemisphere land monsoon and Asian summer monsoon significantly increase by 33.1% and 8.3%, respectively.[37] Here is a logical interpretation of how this intensification of the EASM was driven by remote influences from north Africa. In a greener, less dusty Sahara during the MH, the west African monsoon (WAM) is strengthened.[38] This intensification of the WAM and the northward shift of the intertropical convergence zone (ITCZ) resulted in a decreased upwelling or a warming effect, leading to reduced sea surface temperature (SST) variability in the western equatorial Atlantic.[39] Consequently, the Atlantic Niño phenomenon was triggered, marked by increased precipitation and warmer SSTs in the western Pacific warm pool, a result of a westward shift of the Walker circulation.[40,41] This westward shift of the Walker circulation subsequently drove a northwestward extension and intensification of the western Pacific subtropical high (WPSH) through the Gill-Matsuno response and an intensified local Hadley circulation.[15] This change in the WPSH promotes southerly wind anomalies along the edge of the WPSH, strengthening the prevailing southerly winds over eastern China and prompting a northward shift of the EASM[6,15] (Figure 6A).

It is noticeable that this interpretation, guided by the EC-Earth modeling results, only considers changes in vegetation over northern Africa and its remote impact on EASM. However, proxy archives from the MH point to widespread global vegetation changes, including expanded forest cover in Eurasia and greener conditions in southern and eastern Asia.[42] Therefore, it is plausible that these broader vegetation changes in Europe and Asia could have further influenced the increased rainfall and the northern migration of EASM.

In contrast, the termination of the Green Sahara, characterized by reduced vegetation and increased dust emission, may have triggered an eastward shift in the Walker circulation. This shift could lead to a decrease in the SST over the Indo-Pacific warm pool and a southward migration of the WPSH[3] (Figure 6B). As the WPSH weakens, a strong cyclonic circulation anomaly may hinder the penetration of southerly wind anomalies from the edge of the WPSH into northern China. This would lead to increased precipitation in central and southern China and decreased summer precipitation in northern China.[6,43] However, modern climate dynamics indicate that the onset of the Asian monsoon is typically delayed during El Niño events due to an equatorward contraction of the ITCZ, resulting in overall higher rainfall anomalies in central-eastern China arising from a lengthened Meiyu and a shortened mid-summer stage in northern China.[44,45] Recent modeling experiments have suggested that a strengthened WAM and the subsequent SST changes played a critical role in suppressing the mean state and variability of the El Niño-southern oscillation (ENSO) during the MH.[39] Similarly, a weakened WAM during the end of the Green Sahara could favor ENSO-like conditions, as is evident in the proxies and model simulations.[3]

Rainfall changes over East Asia are closely linked to the south-north displacement of the westerly jet stream.[45,46] The end of the Green Sahara period can also reduce the intensity of the Atlantic meridional overturning circulation, which can

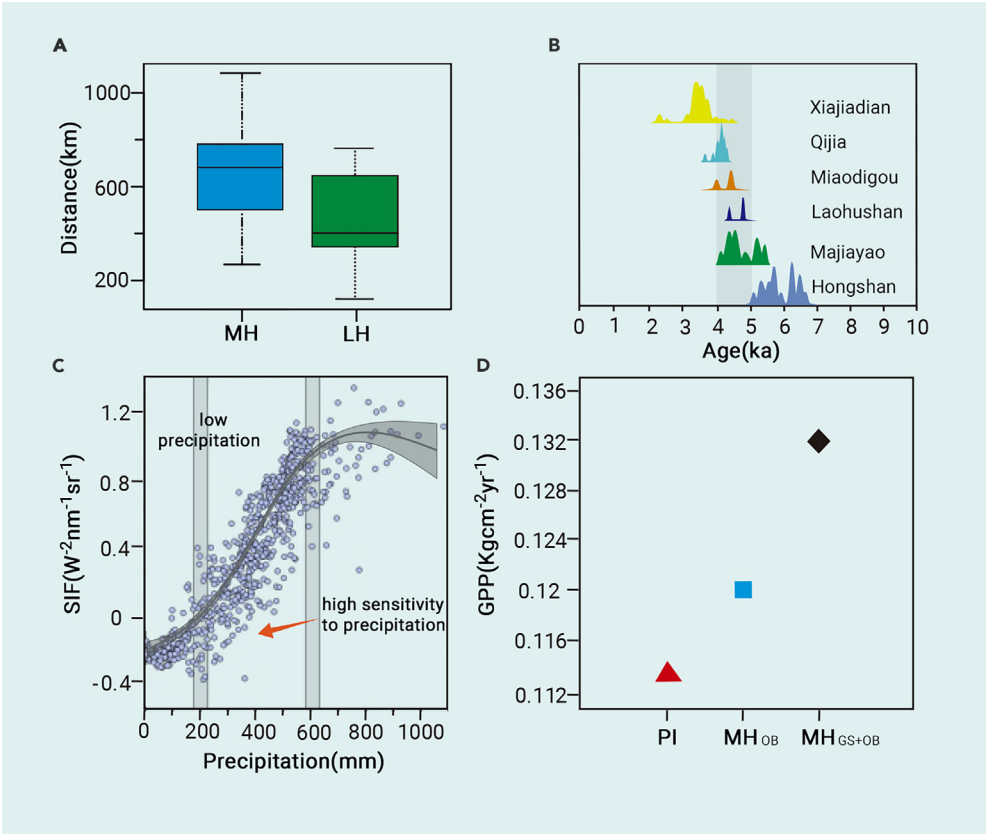

Figure 7. The possible effect of climate change on the late Neolithic culture in northern China (A) The distances between culture relict sites and EASM northern boundary during the MH and LH. The bottom and top of the box represent the 25th and 75th percentiles (the lower and upper quartiles) of distance values, respectively. The band within the box indicates the median of the distances. (B) Density histogram of cultural ^{14}C probability from prehistorical archeological sites; the ^{14}C-dated sites belong to the Xiajiadian, Miaoizgou, Hongshan, Qijian, Laohushan, and Majiayao cultures. (C) Sensitivity analysis of SIF with respect to precipitation amount in northern China. (D) The stimulated GPP values in MH_{GS+OB}, MH_{OB}, and PI. OB, orbital.

cause cooling in the high altitudes of the Northern Hemisphere and intensifying of the mid-latitude westerlies.[47,48] Both observations and model simulations suggested that the southward shift of the westerly jet stream would have prevented the low-level monsoonal flow from penetrating into the interior of East Asia,[46,49] resulting in more rainfalls in central China and a much drier and colder climate in the northern and northwest regions of China.

Impacts of the 5- to 4-ka hydroclimate event on the Neolithic cultural shift in northern China

To comprehend the effect of the environmental transition at 5–4 ka on the late Neolithic culture in northern China, we conducted an analysis of the distances between culture relict sites and the northern boundary of the EASM during the period from 6 to 3 ka. Our findings indicate that these distances were >600 km during the MH, whereas they were nearly halved to ~400 km during the LH (Figure 7A). The MH period, characterized by relatively stable climatic conditions, fostered the growth of rainfed agriculture and provided optimal habitats for Neolithic communities.[50] In contrast, the LH period, due to its proximity to the northern boundary of the EASM, was subjected to increased climate instability, making it highly vulnerable to high-frequency EASM variability and megadrought events. This instability could have caused the collapse of the rainfed culture.

This hypothesis is supported by the observation that culture relict sites were more abundant and endured for a longer duration during the MH as compared to the LH (Figure 7B). For instance, the Hongshan culture thrived from 6.5 to 5.0 ka, spanning a period of 1.5 ka.[9] Similarly, the Yangshao culture flourished during the wet and climatically stable conditions of the MH, extending across China from 7.0 to 5.0 ka.[2] In contrast, the Laohushan culture, a symbol of the Neolithic culture in the Daihai Lake Basin, emerged at ~4.8–4.3 ka but collapsed at ~4.1 ka. This decline was marked by the abandonment of residential sites and migration.[51–53] Moreover, major agriculture-based Neolithic cultures across China's northern boundary experienced nearly simultaneous declines and short-lived episodes after 5.0 ka (Figure 1). For example, in the Liaohe River catchment and northern Hebei Plain, the number of Neolithic sites significantly decreased during the transition from the early Lower Xiajiadian culture (~4.3–4.0 ka) to the Middle Lower Xiajiadian culture (4.0–3.2 ka)[54] (Figure 7B). In the Huangqihai Lake catchment, the culture at the Miaozigou site disappeared at 4.2 ka.[55] The Qijia culture (4.3–3.9 ka) in northwestern China experienced a dramatic population decline and a westward retreat during its late stage.[56] Recent findings also identified the densely distributed Ang'angxi culture (4.5–4.0 ka) in northeastern China during the late Neolithic period.[57]

The Hongshan culture, the first complex society developed in northeastern China, is often considered a distinct culture outside the core regions of early Chinese civilization. It is distinguished by a significant increase in site numbers, the emergence of novel pottery types, and the inception of a highly specialized type of jade work.[58,59] Notable, the jade craftsmanship of the Hongshan culture was remarkably advanced and unique in early China but halted suddenly after 5.0 ka[60] (Figure 7B). At the Niuheliang site, home to the Hongshan culture, the discovery of the earliest leaf-shaped and rectangular stone knives, likely used for harvesting cereal crops, provides evidence that the Hongshan people were early cultivators.[61] These findings provide substantial evidence that the Hongshan culture relied on rainfed agriculture and was highly dependent on precipitation during the growing season.[50] Therefore, it is crucial to examine the relationship between precipitation variability and agriculture productivity, particularly in the geographic context of northern China. In this regard, solar-induced chlorophyll fluorescence (SIF), a proxy for photosynthesis and a robust predictor of cereal crop yield,[62,63] can offer valuable insights. A quantitative analysis of SIF data from 2007 to 2014 across northern China reveals a high sensitivity of cereal crop yield to rainfall changes between 200 and 600 mm (Figure 7C). In present-day conditions, a reduction of ~150 mm in precipitation in northern China could lead to a 20%–30% decrease in terrestrial gross primary productivity (GPP), which directly affects cereal crop yield.

In further explorations, we used dynamic global vegetation models (Lund-Potsdam-Jena General Ecosystem Simulator [LPJ-GUESS]) to perform a set of numerical simulations for the MH and PI periods.[64] The aim is to evaluate how changes in precipitation affect the vegetation composition and distribution in northern China. LPJ-GUESS simulations have shown that during the MH, the forest-steppe ecotone was located between latitudes 36.1°N and 42.3°N (Figure 8B). When the Green Sahara was taken into account, the forest-steppe ecotone shifted further north, with its southern and northern boundaries migrating to 36.5°N and 43.7°N, respectively (Figure 8C). During the PI period, the forest-steppe ecotone shifted southward, with its southern and northern boundary at 36.2°N and 42.2°N, respectively (Figure 8A). These modeling results are consistent with the shift of the forest-steppe ecotone during the Holocene based on pollen reconstruction.[65] In fact, the modeling results also show minimal changes in vegetation types during the PI compared to the MH. However, the vegetation cover, indicating vegetation density, notably decreases from 0.57 to 0.49 during the MH with the inclusion of a Green Sahara and reduced dust (MH_{gsrd}), compared to the PI (Figure 8D). In contrast, the MH simulation without considering Sahara changes indicated a minor change in vegetation cover (0.50–0.49) compared to PI (Figure 8D). Similarly, the mean GPP in modeling simulations was roughly 0.1210 kg C m^{-2} $year^{-1}$ under the MH with a decertified Sahara, similar to the PI condition (0.11471 kg C m^{-2} $year^{-1}$). However, when the Saharan vegetation and less dust were included, the simulated terrestrial GPP increased to 0.1322 kg C m^{-2} $year^{-1}$, which was ~15%

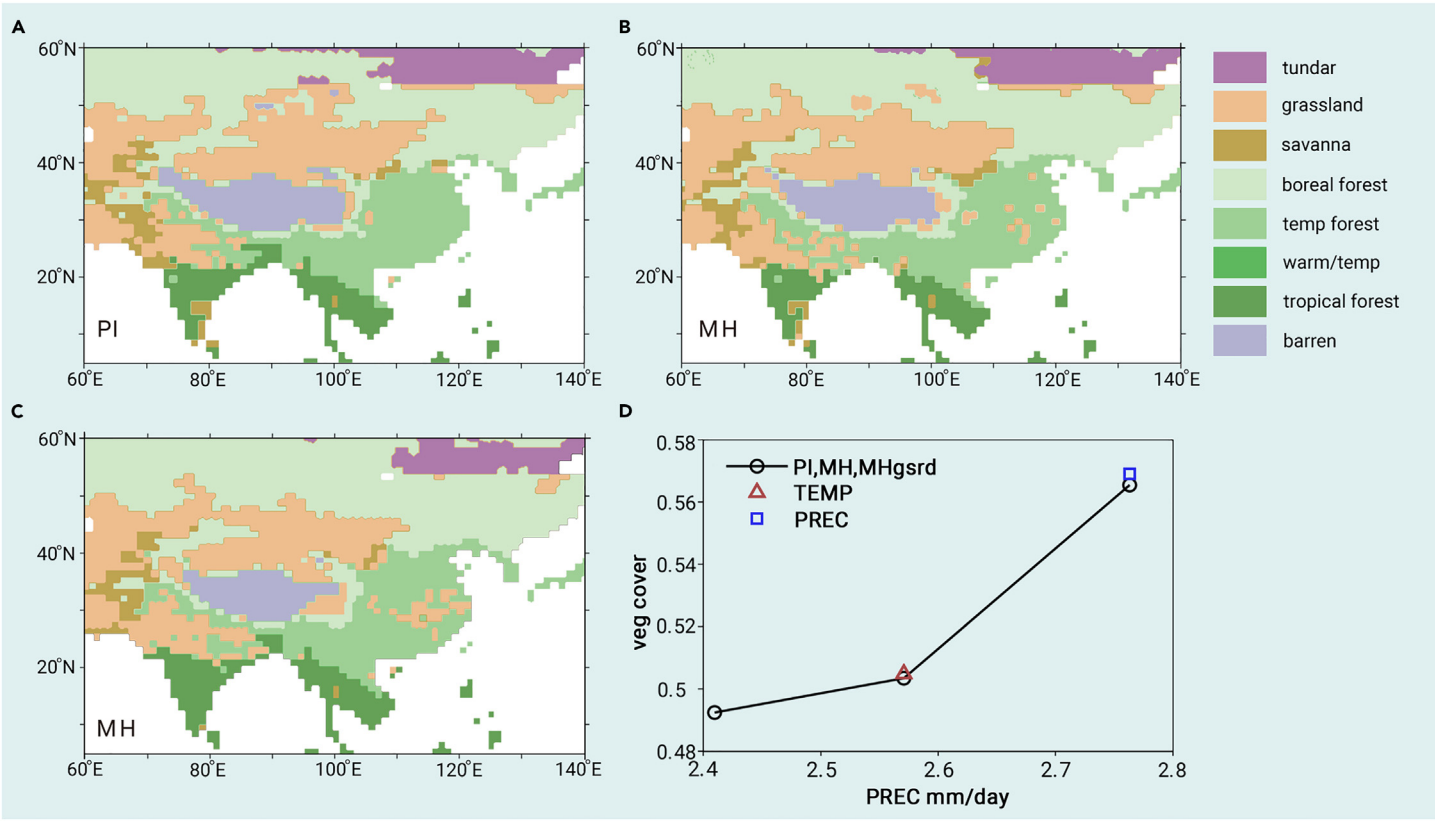

Figure 8. Vegetation distributions and types in simulations Maps of dominant stimulated vegetation types during PI (A), MH (B), and MH_{gsrd} (C), and foliar projective cover (D) over the East Asian.

higher than the PI condition (0.11471 kg C m^{-2} $year^{-1}$) (Figure 7D). This suggests that summer precipitation, which significantly contributes to annual precipitation in northern China,[24] could be a crucial factor. Summer (June, July, August) precipitation anomalies could strongly affect GPP, and this is also supported by the simulated experience (Figure 4B). The considerable reductions in vegetation productivity likely have exacerbated agriculture conditions that are conducive for millet development. For example, millet cultivation nearly vanished in northeastern China while rapidly expanding in the Yellow River Basin during 5.5–4.0 ka, and it reappeared and spread again in northeastern China after 4.0 ka.[66–68] In summary, a southward displacement of 150-mm isohyets during 5–4 ka likely placed a large portion of cultural sites under conditions of drastically reduced vegetation productivity. Subsequent cultures, such as Xiaoheyan culture, were significantly smaller in scale and displayed manufactural techniques compared to the Hongshan culture.[69] The spatial extent and size of archeological sites also largely diminished during the Xiaoheyan culture era.[70]

Numerous studies suggest that a significant environment shift at ~4.2 ka, marked by colder and drier conditions, adversely affected millet farming and prompted southward migration of the population.[1,71] In the turn from 5.0 to 4.0 ka, a decrease occurred in the probability density of millet cultivation, reflecting a decline in millet farming.[67] Despite this, the number of diminished sites continued to increase until the middle of 4 ka, when agricultural activities and population size began to rebound.[13] The unfavorable conditions at the beginning of a fully agricultural lifestyle may have constrained population growth and the spread of millet cultivation in northern China. Subsequent abrupt climate changes shifted the balance toward a pastoral economy, which may have attracted an influx of people already engaged in such practices.[72] The combination of rainfed agriculture and animal husbandry increased the adaptability and resilience of the inhabitants of the region, enabling them to endure the relatively arid conditions at the margins of the monsoonal area in northern China. In essence, the intensification and driving forces of pastoralism in northern China may be linked to these climate changes.

Archeological studies indicate that the spread of West Asian cultural traits, including the cultivation of wheat and barley, as well as the domestication of sheep, goats, and cattle throughout the region, occurred in East Asia during the 5–4 ka.[73] However, the megadrought experienced during this time could have significantly hindered human mobility, potentially limiting or even preventing overland travel between eastern and western Central Asia along the pre–Silk Road between 6 and 5 ka.[73] Stalagmite records from Kyrgyzstan in arid Central Asia (ACA) reveal a prolonged drought during 5.8–5.2 ka,[73] which likely affected the cultural development in ACA and impeded the expansion of cultural traits along oasis routes. The end of the drought event may have prompted the expansion of livestock and facilitated the southward and/or eastward expansion of herdsmen and their livestock from the steppe areas of ACA into northern China.[74] For example, the increased representation of *Sporormiella*-type spores during 5.0–4.0 ka suggests that the herbivore population around Gonghai Lake in northern China was substantially higher compared to the previous periods.[74] Similarly, published accelerator mass spectrometry ^{14}C ages for the remains of the earliest domesticated sheep/goats come from the Youyao site (4.3–4.0 ka),[75] the Jingbianmiaoliang (4.4–4.2 ka) site,[76] and the Hexi Corridor (4.4–3.1 ka).[77] Other dates for sheep or cattle remains have been obtained for the sites of Shimao (4.3–3.8 ka), Muzhuzhuliang (~4.0 ka), and Zhengzemao (~4.8 ka) in Shaanxi Province; Yongxingdian in Zhunger Qi in Inner Mongolia (4.5–4.0 ka); and Dakou (4.2–3.5 ka) and Taosi in Shanxi Province (~4.0 ka).[72]

Our findings suggest that the feedback loops between vegetation, dust, and climate changes from the Sahara may have played a pivotal role in driving societal shifts in northern China through ocean-atmospheric teleconnections. Although alterations in vegetation and dust emission are commonly attributed to climate change induced by variations in Earth's orbit, our research reveals that these changes can themselves feed back into climate systems, significantly influencing monsoon precipitation over northern China. In conclusion, our results also demonstrate that the northern margin of the EASM is strongly affected by Saharan vegetation and dust concentration, with a larger northward migration during the Green Sahara and southward migration at the end of the Green Sahara. This work highlights the sensitivity of the East Asian hydroclimate to large and abrupt shifts in Earth's boundary conditions. Notably, it demonstrates the potential for densely populated regions of East Asia to rapid switch between wet and dry background climate states. However, our findings also provide insights

into a long-term interrelationship between centennial-scale climate change and prehistoric human activities in the EASM region.

MATERIALS AND METHODS

Daihai Lake (40°29′–40°37′N, 112°33′–112°46′E) is a semibrackish closed lake in Inner Mongolia, northern China (Text S1; Figure S1; detailed descriptions in the supplemental information). To reconstruct the lake level, we investigated four outcrops in the western and eastern part of the Daihai Lake basin, respectively (Text S2; Figures S2–S7). Both optically stimulated luminescence (OSL) dating of quartz and post-IR IRSL dating of feldspar were conducted. (Table S1; Text S3; Figures S8–S10). A total of 45 luminescence ages were obtained from all four sections (Table S2). The robustness of the chronology was confirmed by various routine tests (Figures S8–S10). In addition, four radiocarbon samples were taken from three sites and were compared to adjacent luminescence ages (Table S3; Figure 1B). The end-member modeling of grain size extracted diagnostic data from the DH18-3 sequence, such as on provenance, transport, and sedimentation process, which can subsequently be used to reconstruct past climatic variability (Text S4; Figure S11).

The dynamic vegetation model simulations

To elucidate the climate forcing effects on vegetation productivity in northeastern China, we used LPJ-GUESS[64,78] to simulate the gross primary productivity (GPP) in northeastern China in three contrasting past climate scenarios for the MH/LH, the MH Green Sahara (MH_{gsrd}), the MH, and the PI.

LPJ-GUESS simulates structural, compositional, and functional properties of the global ecosystem as influenced by observed or modeled climate conditions and atmospheric carbon dioxide concentrations.[64,78] The spatial resolution of the model is ~1° over the global land surface. This modeling approach has established representations of the past ecosystem evolution in other monsoon regions in good agreement with proxy reconstructions, such as greening in MH western Africa,[79] forest degradation in the MH Amazonia,[80] and vegetation expansion in middle Pliocene Australia.[81]

The PI and MH, and the MH_{gsrd} climate forcings were generated by fully coupled general circulation model simulations using EC-Earth.[38,82] The major difference in boundary conditions between the PI and MH is the seasonal insolation due to precession modulation, with higher summer insolation in the Northern Hemisphere. In MH_{gsrd}, shrub was prescribed and the dust emission was reduced over North Africa, in addition to the model settings in MH, to approximate the MH Green Sahara condition.[83] Therefore, MH_{gsrd} has significantly increased the temperature, and precipitation in northeastern China was primarily driven by stronger summer insolation and remote forcing from land cover changes in North Africa. Two more sensitivity simulations were performed to elucidate the effects of precipitation and temperature on vegetation change in northeastern China. In simulation precipitation, all of the climate forcing variables of the MH were used, except that the precipitation (temperature) values were replaced by those in MH_{gsrd}. More details about these LPJ-GUESS simulations can be found in Lu et al.[81]

REFERENCES

1. Yang, X., Scuderi, L.A., Wang, X., et al. (2015). Groundwater sapping as the cause of irreversible desertification of Hunshandake Sandy Lands, Inner Mongolia, northern China. Proc. Natl. Acad. Sci. USA ***112***, 702–706.
2. Yang, B., Qin, C., Bräuning, A., et al. (2021). Long-term decrease in Asian monsoon rainfall and abrupt climate change events over the past 6,700 years. Proc. Natl. Acad. Sci. USA ***118***, e2102007118.
3. Griffiths, M.L., Johnson, K.R., Pausata, F.S.R., et al. (2020). End of Green Sahara amplified mid- to late Holocene megadroughts in mainland Southeast Asia. Nat. Commun. ***11***, 4204.
4. Wang, Z., Fu, Z., Liu, B., et al. (2022). Northward migration of the East Asian summer monsoon northern boundary during the twenty-first century. Sci. Rep. ***12***, 10066.
5. Wang, B., Liu, J., Kim, H.J., et al. (2012). Recent change of the global monsoon precipitation (1979–2008). Clim. Dyn. ***39***, 1123–1135.
6. Chen, J., Zhang, Q., Huang, W., et al. (2021). Northwestward shift of the northern boundary of the East Asian summer monsoon during the mid-Holocene caused by orbital forcing and vegetation feedbacks. Quat. Sci. Rev. ***268***, 107136.
7. Goldsmith, Y., Broecker, W.S., Xu, H., et al. (2017). Northward extent of East Asian monsoon covaries with intensity on orbital and millennial timescales. Proc. Natl. Acad. Sci. USA ***114***, 1817–1821.
8. Zhang, P., Cheng, H., Edwards, R.L., et al. (2008). A test of climate, sun, and culture relationships from an 1810-year Chinese cave record. Science ***322***, 940–942.
9. Xu, D., Lu, H., Chu, G., et al. (2019). Synchronous 500-year oscillations of monsoon climate and human activity in Northeast Asia. Nat. Commun. ***10***, 4105.
10. Chen, F., Chen, S., Zhang, X., et al. (2020). Asian dust-storm activity dominated by Chinese dynasty changes since 2000 BP. Nat. Commun. ***11***, 992.
11. Li, X.W. (2008). Development of Social Complexity in the Liaoxi Area, Northeast China (Archaeopress).
12. Wang, C., Lu, H., Zhang, J., et al. (2014). Prehistoric demographic fluctuations in China inferred from radiocarbon data and their linkage with climate change over the past 50,000 years. Quat. Sci. Rev. ***98***, 45–59.
13. Leipe, C., Long, T., Sergusheva, E.A., et al. (2019). Discontinuous spread of millet agriculture in eastern Asia and prehistoric population dynamics. Sci. Adv. ***5***, eaax6225.
14. Dong, G., Li, R., Lu, M., et al. (2020). Evolution of human–environmental interactions in China from the late Paleolithic to the Bronze age. Prog. Phys. Geogr. ***44***, 233–250.
15. Piao, J., Chen, W., Wang, L., et al. (2020). Northward extension of the East Asian summer monsoon during the mid-Holocene. Glob. Planet. Change ***184***, 103046.
16. Wu, B., Lang, X., and Jiang, D. (2021). Migration of the northern boundary of the East Asian summer monsoon over the last 21,000 years. JGR. Atmospheres ***126***, e2021JD035078.
17. Chen, J., Huang, W., Jin, L., et al. (2018). A climatological northern boundary index for the East Asian summer and its interannual variability. Sci. China Earth Sci. ***61***, 13–22.
18. Cheng, H., Edwards, R.L., Sinha, A., et al. (2016). The Asian monsoon over the past 640,000 years and ice age terminations. Nature ***534***, 640–646.
19. Yang, S., Ding, Z., Li, Y., et al. (2015). Warming-induced northwestward migration of the East Asian monsoon rain belt from the last glacial maximum to the mid-Holocene. Proc. Natl. Acad. Sci. USA ***112***, 13178–13183.
20. Huang, X., Yang, S., Haywood, A., et al. (2021). Warming-induced northwestward migration of the Asian summer monsoon in the geological past: Evidence from climate simulations and geological reconstructions. JGR. Atmospheres ***126***, e2021JD035190.
21. McGee, D., deMenocal, P., Winckler, G., et al. (2013). The magnitude, timing and abruptness of changes in North African dust deposition over the last 20,000 yr. Earth Planet Sci. Lett. ***371–372***, 163–176.
22. Fu, B.S. (1981). On the calculation of the evaporation from land surface. Scientia Atmos. Sinica ***5***, 23–31.
23. Zhang, L., Hickel, K., Dawes, W.R., et al. (2004). A rational function approach for estimating mean annual evapotranspiration. Water Resour. Res. ***40***, W02502.
24. Xiao, J., Xu, Q., Nakamura, T., et al. (2004). Holocene vegetation variation in the Daihai Lake region of north-central China: a direct indication of the Asian monsoon climatic history. Quat. Sci. Rev. ***23***, 1669–1679.
25. Sun, Q., Wang, S., Zhou, J., et al. (2009). Lake surface fluctuations since the late glaciation at Lake Daihai, North central China: A direct indicator of hydrological process response to East Asian monsoon climate. Quat. Int. ***194***, 45–54.
26. Xu, Q., Xiao, J., Li, Y., et al. (2010). Pollen-based quantitative reconstruction of Holocene climate changes in the Daihai Lake area, Inner Mongolia, China. J. Clim. ***23***, 2856–2868.
27. Xiao, J., Zhang, S., Fan, J., et al. (2019). The 4.2 ka event and its resulting cultural interruption in the Daihai Lake basin at the East Asian summer monsoon margin. Quat. Int. ***527***, 87–93.
28. Long, H., Lai, Z., Fuchs, M., et al. (2012). Timing of Late Quaternary palaeolake evolution in Tengger Desert of northern China and its possible forcing mechanisms. Glob. Planet. Change ***92–93***, 119–129.
29. Wen, R., Xiao, J., Chang, Z., et al. (2010). Holocene precipitation and temperature variations in the East Asian monsoonal margin from pollen data from Hulun Lake in northeastern Inner Mongolia, China. Boreas ***39***, 262–272.
30. Dong, J., Shen, C.C., Kong, X., et al. (2015). Reconciliation of hydroclimate sequences from the Chinese loess plateau and low-latitude East Asian Summer Monsoon regions over the past 14,500 years. Palaeogeogr. Palaeoclimatol. Palaeoecol. ***435***, 127–135.
31. Drysdale, R., Zanchetta, G., Hellstrom, J., et al. (2006). Late Holocene drought responsible for the collapse of Old World civilizations is recorded in an Italian cave flowstone. Geol. ***34***, 101–104.
32. DeMenocal, P., Ortiz, J., Guilderson, T., et al. (2000). Abrupt onset and termination of the African Humid Period: rapid climate responses to gradual insolation forcing. Quat. Sci. Rev. ***19***, 347–361.
33. Thompson, L.G., Mosley-Thompson, E., Davis, M.E., et al. (2002). Kilimanjaro ice core records: evidence of Holocene climate change in tropical Africa. Science ***298***, 589–593.
34. Pennington, B.T., Hamdan, M.A., Pears, B.R., , et al.Sameh, H.I. (2019). Aridification of the Egyptian Sahara 5000–4000 cal BP revealed from x-ray fluorescence analysis of Nile Delta sediments at Kom al-Ahmer/Kom Wasit. Quat. Int. ***514***, 108–118.
35. Tierney, J.E., Russell, J.M., Sinninghe Damsté, J.S., et al. (2011). Late Quaternary behavior of the East African monsoon and the importance of the Congo Air Boundary. Quat. Sci. Rev. ***30***, 798–807.
36. Tierney, J.E., and deMenocal, P.B. (2013). Abrupt shifts in Horn of Africa hydroclimate since the Last Glacial Maximum. Science ***342***, 843–846.
37. Sun, W., Wang, B., Zhang, Q., et al. (2019). Northern Hemisphere land monsoon precipitation increased by the green Sahara during middle Holocene. Geophys. Res. Lett. ***46***, 9870–9879.
38. Pausata, F.S., Messori, G., and Zhang, Q. (2016). Impacts of dust reduction on the northward expansion of the African monsoon during the Green Sahara period. Earth Planet Sci. Lett. ***434***, 298–307.
39. Pausata, F.S.R., Zhang, Q., Muschitiello, F., et al. (2017). Greening of the Sahara suppressed ENSO activity during the mid-Holocene. Nat. Commun. ***8***, 16020.
40. Rodríguez-Fonseca, B., Polo, I., García-Serrano, J., et al. (2009). Are Atlantic Niños enhancing Pacifc ENSO events in recent decades? Geophys. Res. Lett. ***36***, L20705.
41. Li, X., Xie, S.P., Gille, S.T., et al. (2016). Atlantic-induced pan-tropical climate change over the past three decades. Nat. Clim. Chang. ***6***, 275–279.
42. Pausata, F.S.R., Messori, G., Yun, J., et al. (2021). The remote response of the South Asian Monsoon to reduced dust emissions and Sahara greening during the middle Holocene. Clim. Past ***17***, 1243–1271.
43. Sun, Y., Clemens, S.C., Morrill, C., et al. (2012). Influence of Atlantic Meridional overturning circulation on the East Asian winter monsoon. Nat. Geosci. ***5***, 46–49.

44. Berry, G., and Reeder, M.J. (2014). Objective identification of the intertropical convergence zone: Climatology and trends from the ERA-Interim. J. Clim. ***27***, 1894–1909.
45. Zhang, H., Griffiths, M.L., Chiang, J.C.H., et al. (2018). East Asian hydroclimate modulated by the position of the westerlies during Termination I. Science ***362***, 580–583.
46. Chiang, J.C., Fung, I.Y., Wu, C.H., et al. (2015). Role of seasonal transitions and westerly jets in East Asian paleoclimate. Quat. Sci. Rev. ***108***, 111–129.
47. Chiang, J.C., Lee, S.Y., Putnam, A.E., et al. (2014). South Pacific Split Jet, ITCZ shifts, and atmospheric North-South linkages during abrupt climate changes of the last glacial period. Earth Planet Sci. Lett. ***406***, 233–246.
48. Zhang, M., Liu, Y., Zhang, J., et al. (2021). AMOC and Climate Responses to Dust Reduction and Greening of the Sahara during the Mid-Holocene. J. Clim. ***34***, 4893–4912.
49. Herzschuh, U., Cao, X., Laepple, T., et al. (2019). Position and orientation of the westerly jet determined Holocene rainfall patterns in China. Nat. Commun. ***10***, 2376.
50. Guo, L., Xiong, S., Ding, Z., et al. (2018). Role of the mid-Holocene environmental transition in the decline of late Neolithic cultures in the deserts of NE China. Quat. Sci. Rev. ***190***, 98–113.
51. Tian, G.J., and Akiyama, S. (2001). Archaeological Excavations at Daihai (II) – A Collection of Sino-Japanese Reports and Papers on Sites in Daihai (Science Press). (in Chinese).
52. Tian, G.J. (2000). The relationships between archaeological culture and ecological environment in Daihai Lake area. In Research of Environmental Archaeology (Part 2), K.S. Zhou and Y.Q. Song, eds. (Science Press), pp. 72–80. (in Chinese).
53. Fang, X.Q., and Sun, N. (1998). Cold event: a possible cause of the interruption of the Laohushan Culture. Hum. Geogr. ***13***, 71–76.
54. Tarasov, P., Jin, G., and Wagner, M. (2006). Mid-Holocene environmental and human dynamics in northeastern China reconstructed from pollen and archaeological data. Palaeogeogr. Palaeoclimatol. Palaeoecol. ***241***, 284–300.
55. Huang, Y.P. (2003). Miaozigou yu Dabagou yizhi dongwu yihai jianding baogao. In Wenwu Kaogu Yanjiusuo, Neimenggu, Y.D. Miaozigou, ed. (Encyclopedia of China Publishing House), pp. 599–611.
56. Liu, F., and Feng, Z. (2012). A dramatic climatic transition at similar to 4000 cal. yr BP and its cultural responses in Chinese cultural domains. Holocene ***22***, 1181–1197.
57. Heilongjiang Institute of Cultural Relics and Archaeology (2020). Archaeological Excavations at Honghe Site–A Site Report on Ang'angxi Culture. Archaeology ***7***, 20–33.
58. Liu, L., and Chen, X.C. (2012). The Archaeology of China: From the Late Paleolithic to the Early Bronze Age (Cambridge University Press).
59. Drennan, R.D., Peterson, C.E., Lu, X.M., et al. (2017). Hongshan households and communities in Neolithic northeastern China. J. Anthropol. Archaeol. ***47***, 50–71.
60. Anderson, D.C. (2012). Hongshan Jade Treasures: The Art, Iconography and Authentication of Carvings from China's Finest Neolithic Culture (Tau Publishing, Fraz. Pian diPorto).
61. Mo, D.W., Wang, H., and Li, S.C. (2003). Effects of Holocene environmental changes on the development of archaeological cultures in different regions of North China. Quat. Sci. ***23***, 200–210.
62. Zan, M., Zhou, Y., Ju, W., et al. (2018). Performance of a two-leaf light use efficiency model for mapping gross primary productivity against remotely sensed sun-induced chlorophyll fluorescence data. Sci. Total Environ. ***613–614***, 977–989.
63. Sinha, A., Kathayat, G., Weiss, H., et al. (2019). Role of climate in the rise and fall of the neo-Assyrian empire. Sci. Adv. ***5***, eaax6656.
64. Smith, B., Wårlind, D., Arneth, A., et al. (2014). Implications of incorporating N cycling and N limitations on primary production in an individual-based dynamic vegetation model. Biogeosciences ***11***, 2027–2054.
65. Cheng, Y., Liu, H., Dong, Z., et al. (2020). East Asian summer monsoon and topography co-determine the Holocene migration of forest-steppe ecotone in northern China. Glob. Planet. Change ***187***, 103135.
66. Jia, X., Sun, Y., Wang, L., et al. (2016). The transition of human subsistence strategies in relation to climate change during the Bronze Age in the West Liao River Basin, Northeast China. Holocene ***26***, 781–789.
67. Hosner, D., Wagner, M., Tarasov, P.E., et al. (2016). Spatiotemporal distribution patterns of archaeological sites in China during the Neolithic and Bronze Age: An overview. Holocene ***26***, 1576–1593.
68. Wang, J., Zhou, X., Xu, H., et al. (2021). Relationship between C_4 biomass and C_4 agriculture during the Holocene and its implications for millet domestication in Northeast China. Geophys. Res. Lett. ***48***, e2020GL089566.
69. Deng, H. (1997). The change of then man-land relationship in the northern Yanshan Mountain in region during megathermal. Acta Geograph. Sin. ***52***, 163–171.
70. Shelach-Lavi, G., Teng, M., Goldsmith, Y., et al. (2016). Human adaptation and socioeconomic change in northeast China: results of the Fuxin regional survey. J. Field Archaeol. ***41***, 467–485.
71. Sun, Q., Liu, Y., Wünnemann, B., et al. (2019). Climate as a factor for Neolithic cultural collapses approximately 4000 years BP in China. Earth Sci. Rev. ***197***, 102915.
72. Zhang, Y., Zhang, Y., Hu, S., et al. (2021). Pastoralism and millet cultivation during the Bronze Age in the temperate steppe region of Northern China. Front. Earth Sci. ***9***, 748327.
73. Tan, L., Dong, G., An, Z., et al. (2021). Megadrought and cultural exchange along the proto-silk road. Sci. Bull. ***66***, 603–611.
74. Huang, X., Zhang, J., Ren, L., et al. (2021). Intensification and Driving Forces of Pastoralism in Northern China 5.7 ka Ago. Geophys. Res. Lett. ***48***, e2020GL092288.
75. Dodson, J., Dodson, E., Banati, R., et al. (2014). Oldest Directly Dated Remains of Sheep in China. Sci. Rep. ***4***, 7170.
76. Hu, S.M. (2021). The Development of Animal Husbandry from the Perspective of Archaeology in Yulin Area-Based on the Animal Archaeology and the Latest Dating Data from 5000-4000 Years Ago in Yulin Area (Chinese Journal of Social Science Special issue of National Social Science Foundation).
77. Yang, Y., Ren, L., Dong, G., et al. (2019). Economic Change in the Prehistoric Hexi Corridor (4800-2200 BP), Northwest China. Archaeometry ***61***, 957–976.
78. Smith, B., Prentice, I.C., and Sykes, M.T. (2001). Representation of vegetation dynamics in the modelling of terrestrial ecosystems: comparing two contrasting approaches within European climate space. Glob. Ecol. Biogeogr. ***10***, 621–637.
79. Lu, Z., Miller, P.A., Zhang, Q., et al. (2018). Dynamic vegetation simulations of the mid-Holocene Green Sahara. Geophys. Res. Lett. ***45***, 8294–8303.
80. Kukla, T., Ahlström, A., Maezumi, S.Y., et al. (2021). The resilience of Amazon tree cover to past and present drying. Glob. Planet. Change ***202***, 103520.
81. Lu, Z., Miller, P.A., Zhang, Q., et al. (2019). Vegetation pattern and terrestrial carbon variation in past warm and cold climates. Geophys. Res. Lett. ***46***, 8133–8143.
82. Hazeleger, W., Wang, X., Severijns, C., et al. (2012). EC-Earth V2. 2: description and validation of a new seamless earth system prediction model. Clim. Dyn. ***39***, 2611–2629.
83. Claussen, M., Dallmeyer, A., and Bader, J. (2017). Theory and modeling of the African humid period and the green Sahara. In Oxford Research Encyclopedia of Climate Science.

ACKNOWLEDGMENTS

This research was supported by the National Key Research and Development Program of China (no. 2022YFF0801103), the Strategic Priority Research Program of the Chinese Academy of Sciences (no. XDB40010200), the National Natural Science Foundation of China (no. 41977381), and the Youth Innovation Promotion Association CAS (grant no. Y201959). The EC-Earth and LPJ-GUESS simulations were performed on the Swedish National Infrastructure for Computing at the National Super-computer Center, partially funded by the Swedish Research Council through grant agreement no. 2018-05973. We thank Lili Liu for the laboratory work, Yingxiao Yu for the field sampling, and Yunkai Zhou for providing the meteorological data.

AUTHOR CONTRIBUTIONS

H.L. designed and organized this study. Y.H., H.L., and Q.Z. wrote the draft manuscript. S.T., M.F., T.T., L.G., J.Z., and J.S. analyzed the data. I.D. performed the water balance model. Z.L., J.C., Q.Z., and W.S. performed the simulation experiments. All of the authors contributed to the discussions and revisions for the manuscript.

DECLARATION OF INTERESTS

The authors declare no competing interests.

SUPPLEMENTAL INFORMATION

It can be found online at https://doi.org/10.1016/j.xinn.2023.100550.

LEAD CONTACT WEBSITE

http://sourcedb.niglas.cas.cn/zw/rck/201511/t20151124_4473218.html